

Characterization and Optimization of a Cryogenic Pure CsI Detector with Remarkable Light Yield and Unprecedented Energy Resolution for CLOVERS Experiment*

Chen-Guang Su,¹ Qian Liu,^{1,†} Ling-Quan Kong,¹ Chen Shi,¹ Kimiya Moharrami,¹ Yang-Heng Zheng,¹ and Jin Li¹

¹*School of Physical Sciences, University of Chinese Academy of Sciences, Beijing, 100049, China*

In this study, we conducted a comprehensive characterization and optimization of a cryogenic pure CsI (pCsI) detector. We utilized a 2 cm cubic crystal coupled with a HAMAMATSU R11065 photomultiplier tube (PMT), achieving a remarkable light yield of 35.2 PE/keV_{ee} and an unprecedented energy resolution of 6.9% at 60 keV. Additionally, we measured the scintillation decay time of pCsI, which proved to be significantly faster than that of CsI(Na) at room temperature. Furthermore, we investigated the impact of temperature, surface treatment, and crystal shape on the light yield. Notably, the light yield peaked at approximately 20 K and remained stable within the range of 70 – 100 K. We observed that the light yield of polished crystals was approximately 1.5 times greater than that of ground crystals, while the crystal shape exhibited minimal influence on the light yield. These results are crucial for the design of the 10 kg pCsI detector for the future CLOVERS (Coherent eLastic neutrino(V)-nucleus scattERING at China Spallation Neutron Source (CSNS)) experiment.

Keywords: Cryogenic CsI detector; Light yield; Energy resolution; Scintillation decay time; Light yield optimization; CLOVERS; CE ν NS;

DOI:

I. INTRODUCTION

The Coherent Elastic Neutrino-Nucleus Scattering (CE ν NS) process has garnered lots of attention since its first detection in 2017 by COHERENT collaboration [1]. Owing to the coherent enhancement of the cross section (2-3 orders higher than any other neutrino matter interaction process with neutrino energy below 100 MeV) and nearly pure electromagnetic-weak dynamics (cross section easy to calculate), it serves as a valuable probe and novel neutrino detection method. As a probe, with precise cross section measurement, it examines the Standard Model at low momentum transfer, aids astrophysics in understanding core-collapsed supernova bursts [2, 3], helps to determine the neutron radius of nucleus [4], and clarifies the neutrino fog in WIMP dark matter searches like CDEX and PandaX experiments [5, 6]. As a new neutrino detection method, it offers a flavor-independent approach to search for sterile neutrinos, a sensitive detection of solar and supernova neutrinos, and a threshold-free way to measure the reactor neutrino spectrum below the 1.8 MeV IBD threshold, which would be highly valuable to reactor oscillation experiment like JUNO [7]. However, the typical observable ionization energy of the recoiled nucleus is only around 1 keV electron-equivalent (keV_{ee}), making signal detection highly challenging. Various technologies have been proposed to detect CE ν NS signals. For instance, the RELICS project plan to utilize Liquid

Xenon detectors [8], while the RECODE experiment have opted for HPGe detectors [9].

To precisely measure the cross section of the CE ν NS process and advance detector technology based on CE ν NS, we propose the CLOVERS (Coherent eLastic neutrino(V)-nucleus scattERING at China Spallation Neutron Source (CSNS)) experiment [10, 11]. Cryogenic pure CsI (pCsI) detectors are adopted due to their large cross section, proportional to the square of the neutron number in the nucleus [12], and high light yield, reaching 33.5 photo – electrons(PE)/keV_{ee} coupled to photomultiplier tube (PMT) [13] and 43.0 PE/keV_{ee} coupled to Silicon photomultiplier (SiPM) [14]. To better understand and enhance the cryogenic pCsI detector's performance, detailed characterization and optimization has been conducted. In this work, the light yield, energy resolution, and scintillation decay time of pCsI crystal at 77K has been characterized. The influence of temperature, crystal shape, and crystal surface treatment on the light yield was also investigated. A world-leading energy resolution for scintillator detectors has been achieved and a direction for optimizing future CLOVERS 10 kg pCsI detectors has been identified.

II. EXPERIMENTAL SETUP

The experimental setup for this study is depicted in Fig.1. The pCsI crystals, obtained from HAMAMATSU BEIJING, come in two different shapes: 2×2×2 cm³ cubes and Φ 2.5×2 cm³ cylinders. The light output surfaces of all crystals were polished, while the remaining surfaces varied between being ground or polished depending on the specific crystal. The R_a was around 40 nm for polished surfaces and around 800 nm for ground surfaces.

A ²⁴¹Am radioactive source was affixed to a side surface of the crystal. Signals generated by its 10 – 30 keV X-rays and 60 keV gamma are used for the characterization and op-

* This work was supported by the National Key R&D Program of China 2022YFA1602204, the National Natural Science Foundation of China (Grant Nos. 12175241, 12221005), the Fundamental Research Funds for the Central Universities, the International Partnership Program of the Chinese Academy of Sciences under Grant No. 211134KYSB20200057 and the Double First-Class University Project Foundation of USTC. The authors thank Hefei Comprehensive National Science Center for their strong support.

† Corresponding author, Qian Liu, liuqian@ucas.ac.cn, +8618910949066

timization of the detector. The crystal was directly coupled to the quartz window of a HAMAMATSU R11065 3-inch PMT without the use of any optical coupling grease or silicon rubber. To minimize light leakage, the side and bottom surfaces of the crystal, as well as the remaining area of the PMT window, were enveloped in four layers of Luxiumsolutions BC-642 Teflon reflection material. Springs were employed to press the PMT window against the light output surface of the crystal, ensuring adequate optical contact between the PMT and crystal, as well as thermal contact between the crystal and the copper pedestal coupled to the cooling platform using cryogenic vacuum silicone thermal grease.

The cryogenic system comprised a custom vacuum chamber, an Agilent TPS-mini molecular pump, a CryoPride KDC6000V helium compressor, and a CryoPride KDE401SA refrigerating machine, capable of achieving a vacuum pressure below 1×10^{-6} Pa and a temperature as low as 3 K. Temperature control and monitoring were carried out using a Lake Shore Model 325.

The R11065 PMT was powered by a CAEN NDT1470 HV module with a negative high voltage of 1500V. The PMT signal was read out by a CAEN DT5751 digitizer with a 1 GHz sampling rate, 500 MHz bandwidth, 1 Vpp dynamic range, and 10 bit resolution. The working mode of DT5751 was set to self-trigger and the trigger threshold was 30 ADC counts. The original waveform data were directly recorded in CERN ROOT format using a modified WaveDump software[15, 16].

III. DATA ANALYSIS

A typical signal waveform induced by a 60 keV gamma from ^{241}Am in pCsI at 77 K is shown in Fig.2. Each waveform consists of 8000 samples, corresponding to a duration of 8000 ns given the 1 GHz sampling rate of DT5751.

To analyze the waveforms, a toolkit based on C++ and CERN ROOT has been developed [17], implementing the following algorithm:

1. The waveform is divided into two regions: the baseline (BL) region covering samples 0-1399 and the signal (SG) region covering samples 1400-7999.
2. In the BL region, the mean value (μ_{BL}) and standard deviation (σ_{BL}) of the baseline for each waveform is decided.
3. Next, the baseline of the waveform is adjusted to 0, and the waveform is inverted.
4. A peak-searching algorithm to identify all peaks in the SG region is applied. A peak is identified when a sample deviates from 0 by at least $5\sigma_{BL}$. This sample is defined as the trigger point. The start (T_S) and end (T_E) of each peak are defined by the first sample falling back to 0 backwards and forwards from the trigger point, as illustrated in the subplot of Fig.2.
5. The integral of the ADC numbers of each peak is recorded in a C++ std::vector named *PeakQ* for each

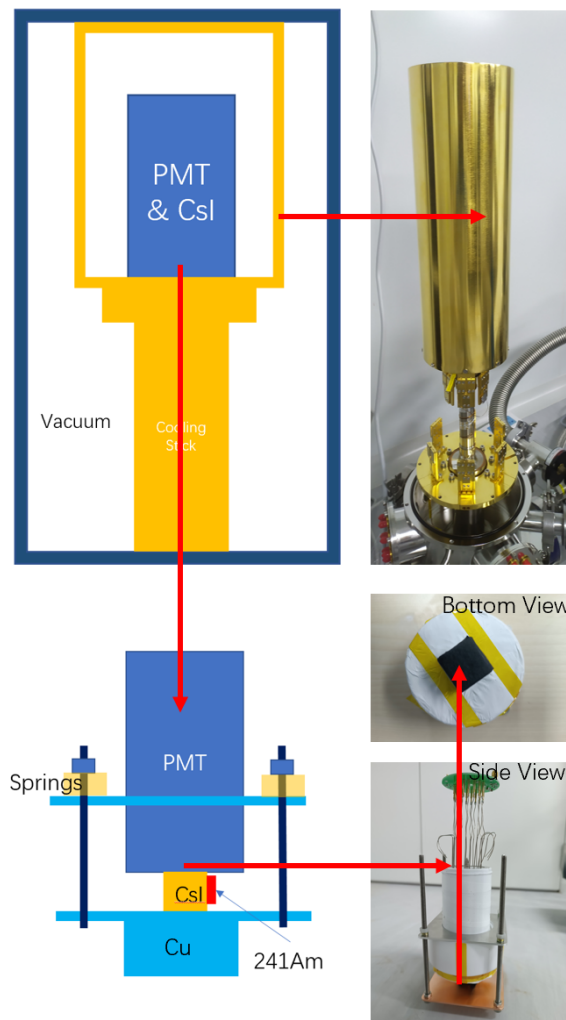


Fig. 1. Schemes and pictures of the experimental setup. A 2 cm cubic pCsI crystal is directly coupled to a HAMAMATSU R11065PMT by springs, wrapped by four layers of BC-642 Teflon tape.

event. The total charge, i.e., the sum of all elements in *PeakQ*, is stored as a C++ float variable named *TotalQ* for each event. These variables are utilized to derive the results in subsequent analyses.

IV. CHARACTERIZATION OF PCSI DETECTOR AT 77 K

Using the setup and analysis method described in sec.II and sec.III, the light yield, energy resolution and scintillation decay time of pCsI detector at 77 K has been measured. The crystal used in this characterization was a $2 \times 2 \times 2$ cm³ cube and all its surfaces were polished.

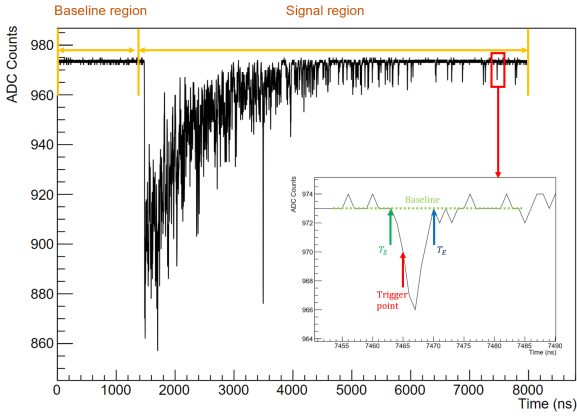


Fig. 2. A typical signal waveform induced by ^{241}Am 60 keV gamma for pCsI at 77 K. The subplot shows the process of peak searching.

A. Single PE calibration of the PMT

To determine the light yield of the pCsI detector, a single photoelectron (SPE) calibration is necessary. An online SPE calibration is conducted by populating a histogram (Fig.3) with the *PeakQ* of peaks with T_S between 7000 and 7999 ns for all events in dataset. As depicted in Fig.2, within the 7000-7999 ns range, the peaks are sparse, with each likely corresponding to an SPE. The subplot illustrates a typical SPE signal. Given the small contribution from multi-PE events, the histogram in Fig.3 is fitted using a simplified SPE model, similar to the one described in Ref.[18].

$$f(q) = [Bkg(q) + \sum_{i=1}^3 a_i g_i(q, Q_{spe}, \sigma_{spe})] \times Acp(q) \quad (1)$$

where

$$Bkg(q) = a_{bkg} \cdot e^{-\frac{q}{\sigma_{bkg}}} \quad (2)$$

$$g_i(q) = a_i \cdot \text{Gaus}(q, iQ_{spe}, \sqrt{i}\sigma_{spe}) \quad (3)$$

$$Acp(q) = [1 + e^{-k(q-q_0)}]^{-1} \quad (4)$$

The $Bkg(q)$ term describes events generated by electrons emitted from dynodes undergoing incomplete multiplication. The $g_i(q)$ terms represent the i -PE Gaussian response for fully multiplied electrons. Q_{spe} is the mean SPE charge and σ_{spe} represents the spread of SPE charge due to the fluctuation in the PMT multiplication process. The $Acp(q)$ term is a sigmoid-shaped function describing the threshold effect introduced by the peak searching algorithm discussed in Sec.III. q_0 represents the edge midpoint and k controls the steepness of the edge. The a_i values are not constrained to a Poisson distribution since the process of populating *PeakQ* into this histogram is not a Poisson procedure.

The fitted curve is depicted in Fig.3. The fitted results are: $Q_{spe} = 32.50(3)$ and $\sigma_{spe} = 10.37(3)$ in units of ADC counts·ns.

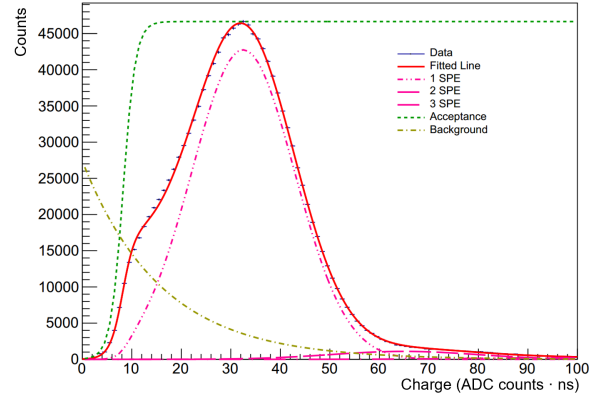


Fig. 3. SPE histogram filled by *PeakQ* of peaks with T_S in range 7000-7999 ns. A simplified SPE model is fitted to the histogram. $\mu_{spe} = 32.50 \pm 0.03$ and $\sigma_{spe} = 10.37 \pm 0.03$ in unit of ADC counts·ns

B. Light yield and energy resolution of pCsI

The recorded energy spectrum of ^{241}Am , measured in terms of the number of photoelectrons (NPE) generated in each event, is illustrated in Fig.4. The NPE is computed using the following formula:

$$NPE = \frac{\text{Total}Q}{Q_{spe}} \quad (5)$$

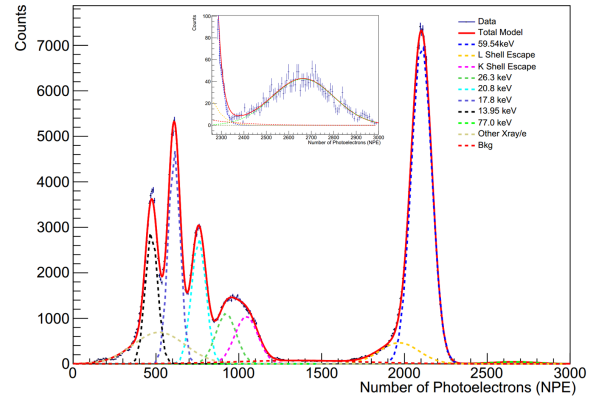


Fig. 4. Energy spectrum of ^{241}Am measured by pCsI detector at 77K. 10 unconstrained Gaussian functions are used for the global fitting of the spectrum. The fitted curve and its components are shown.

The spectrum undergoes a global fit employing 10 unconstrained Gaussian functions to accommodate various components. The 59.54 keV and 26.3 keV gamma peaks originate from intrinsic gamma rays emitted during ^{241}Am decay. K Shell Escape and L Shell Escape peaks are unique to CsI detectors due to X-rays or Auger electrons' delayed release or escape after a 59.54 keV gamma ejects a K or L shell electron in cesium (Cs) or iodine (I) atoms. The 13.95 keV, 17.8 keV, and 20.8 keV X-rays stem from activated states of ^{237}Np , a decay product of ^{241}Am . These peaks are merged

due to nearby X-rays rather than being monotonous X-rays. The 77 keV peak arises from the coincidence of 59.54 keV gamma and X-rays. A Bkg component accounts for events from environmental radioactive background. Additionally, an Other X-ray/e component addresses the complex X-ray and electron spectrum below 25 keV, necessitating more than three Gaussian functions.

The fitted curve and its components are depicted in Fig.4, with details listed in Tab.1. The detector's light yield (LY) at various energy points is calculated using:

$$LY[NPE/keV_{ee}] = \frac{\mu_{npe}}{Energy[keV_{ee}]} \quad (6)$$

where μ_{npe} denotes the Gaussian's fitted mean at a given energy point.

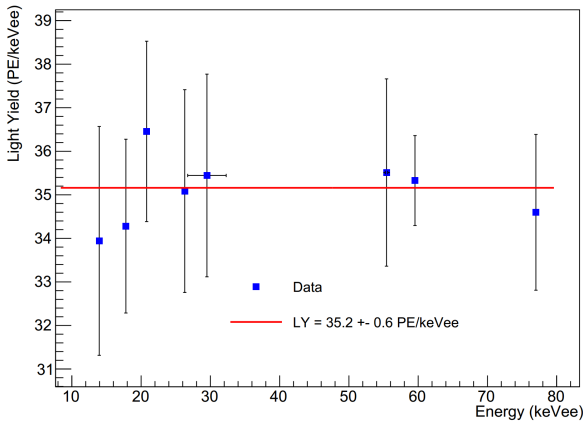


Fig. 5. Light yield calculated at different energy points and their averaged value.

The light yield results obtained at various energy points were fitted using a zero-order polynomial function to determine the mean light yield along with associated uncertainties. The fitted outcome is illustrated in Fig.5. The error bars depicted on the graph represent the standard deviation of the Gaussian function fitted at different energy points. The final mean light yield of this pCsI detector at 77 K is 35.2(6) PE/keV_{ee}, slightly higher than the assumed value utilized in CLOVERS sensitivity estimation, 33.5(7) PE/keV_{ee}, as reported by Ref.[13], where the CsI crystal was also coupled to an R11065 PMT.

The most remarkable achievement in this study is the outstanding and world-leading energy resolution attained for scintillator detectors. Given that the 60 keV gamma peak is monotonic (unlike X-rays, K/L Shell escape, and coincidence peaks) and less influenced by nearby peaks (unlike the 26.3 keV gamma peak, strongly affected by nearby X-rays and K shell escape peaks), its resolution is chosen to represent the overall resolution of this study. The full width at half maximum (FWHM) energy resolution of this pCsI detector at 77 K at 60 keV has reached 6.9%, surpassing the reported 9.5% in Ref.[13], 8.8% in Ref. [?] and 7.8% in Ref.[20], making it the best among all the reported resolutions of cryogenic pCsI detectors. This resolution even outperforms that

of the brightest inorganic scintillators typically used at room temperature, such as NaI(Tl), CsI(Na), CsI(Tl) or LaBr₃. A summary of this comparison is presented in Fig.6.

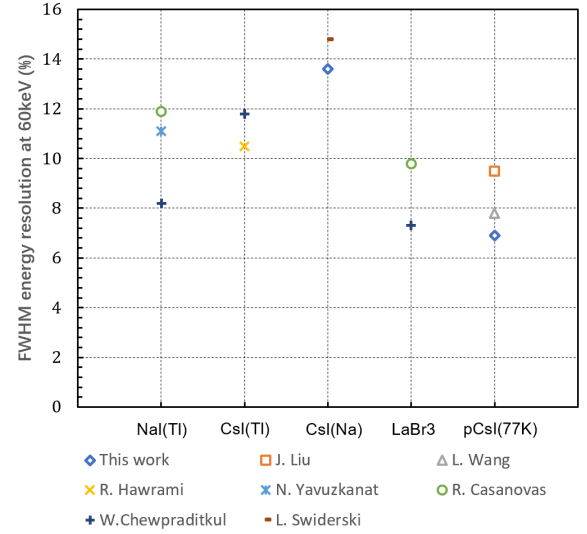


Fig. 6. Comparison of energy resolution at 60 keV of different crystals from various studies reveals that the 6.9% resolution achieved in this work by the pCsI detector at 77 K is superior to all others. Resolution data were obtained from J. Liu[13], L. Wang[20], R. Hawrami[21], N. Yavuzkanat[22], R. Casanovas[23], W. Chewpraditkul[24], and L. Swiderski[25].

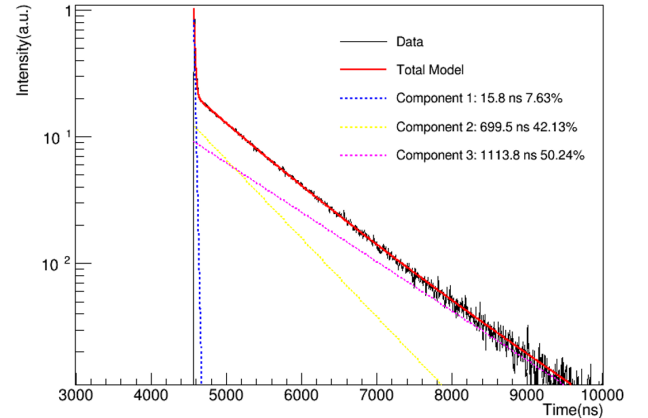


Fig. 7. The scintillation decay time fitting of the pCsI detector at 77 K. The waveform fitted is the sum of 100k ²⁴¹Am induced events and normalized to its maximum value. The decay constants and composition fractions of different components are listed

C. Scintillation decay time of pCsI

The scintillation decay time of the pCsI detector at 77 K was determined by fitting the accumulated and normalized waveform with three exponential components. The waveform and fitted results are shown in Fig.7. The decay time

Table 1. Fitted results of the measured ^{241}Am spectrum

Type	Energy(keV _{ee})	μ_{npe}	σ_{npe}	LY(NPE/keV _{ee})	FHWM (%)
γ	59.54	2103.4	61.46	35.3	6.9
L shell escape	55.43*	1968.4	119.2	35.5	14.3
K shell escape	29.5*	1045.6	68.7	35.4	15.5
γ	26.3	922.8	61.2	35.1	15.6
X-ray	20.8†	758.3	43.1	36.5	13.4
X-ray	17.8†	610.2	35.5	34.3	13.7
X-ray	13.95†	473.5	36.7	33.9	18.2
Coincidence	77.3	2664.0	137.7	34.5	12.2

* Averaged among Cs and I atoms[19]. † Mean energy of X-rays nearby [19].

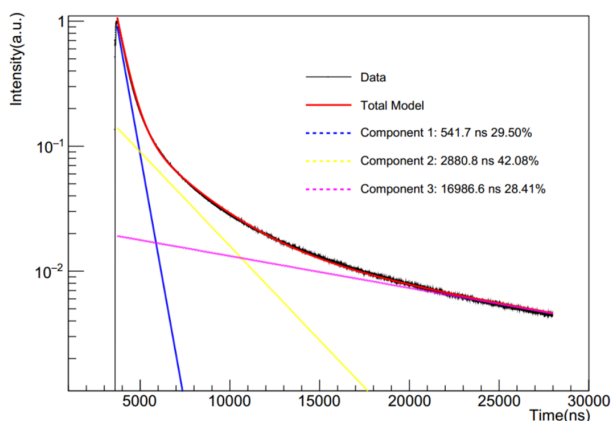


Fig. 8. The scintillation decay time fitting of the CsI(Na) detector at room temperature followed the same setup as the pCsI experiment, except for the crystal type.

of the slowest component of pCsI at 77 K is approximately $1 \mu\text{s}$, much faster than that of CsI(Na) crystal, which is around $17 \mu\text{s}$, as depicted in Fig.8. These results are consistent with other experiments. [26–28]. The considerably shorter decay time of pCsI will significantly reduce the afterglow background induced by environmental radioactive events, which contaminates around 30% of all the events in the COHERENT CsI(Na) experiment. [18].

V. OPTIMIZATION OF CRYOGENIC PCSI DETECTOR

To optimize the performance of the cryogenic pCsI detector, investigations were conducted to assess the influence of temperature, surface treatment, and crystal shape on the light yield.

A. Influence of temperature on the light yield

The relative light yields of the pCsI detector at different temperatures are depicted in Fig.9, alongside results from V. Mikhailik [29], C. Amsler [30], and X. Zhang [31]. The results from this study and V. Mikhailik are normalized to the maximum value in each dataset. However, the results from C.

Amsler and X. Zhang do not include data points below 77 K, so their light yields are normalized to the value in this study at 77 K based on their results at the same temperature. All results show good agreement in the overall trend, with slight differences in details possibly due to variations in PMT setup and crystal used.

The light yield increases rapidly as the temperature is cooled down from room temperature to around 100 K. Then, it reaches a plateau between 70 K and 100 K, followed by a slight increase at around 60 K. The maximum light yield is attained at around 20 K, after which it drops rapidly as the temperature decreases, consistent with both our results and those of V. Mikhailik. Although there is a 20% increase in light yield from 77 K to 20 K, cooling down to 20 K is considerably more challenging than cooling to 77 K, which can be easily achieved with inexpensive and relative safe liquid nitrogen.

Since the light yield remains relatively stable between 70 K and 100 K, another potential approach is to place the pCsI in a 87 K liquid argon environment and utilize the liquid argon as an active veto system to reject background introduced by external particles such as neutrons or gammas.

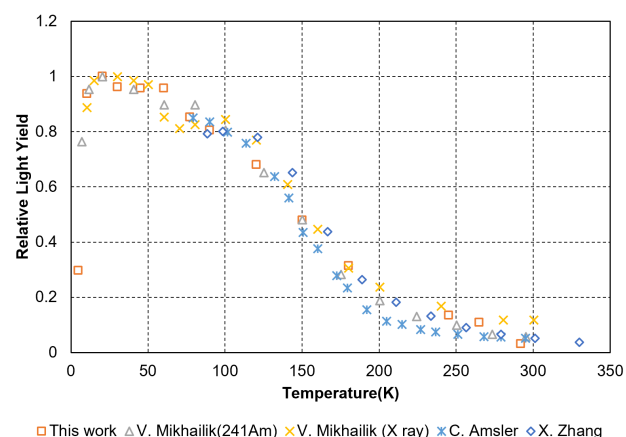


Fig. 9. The relative light yield at various temperatures from multiple datasets shows consistent agreement in the overall trend. Both this study and V. Mikhailik's results indicate that the maximum light yield is achieved around 20 K. The results from V. Mikhailik are sourced from Ref.[29], C. Amsler's from Ref.[30], and X. Zhang's from Ref.[31].

B. Influence of surface treatment on the light yield

In addition to temperature, another factor that could influence the light yield is the surface treatment of the crystal, affecting the light collection efficiency of the detector system, as mentioned in Ref.[32], Ref.[33] and Ref.[34]. To optimize the selection of surface treatment (ground or polished), four comparison experiments were conducted.

Experiment A aimed to compare the light yield of two cubic crystals with different surface treatments. One crystal had all its surfaces polished, while the other had surfaces ground except for the light output surface. The ratio between the light yield of the ground and polished crystal, R_{ly} , is defined as:

$$R_{ly} = \frac{LY_{ground}}{LY_{polished}} \quad (7)$$

This comparison was conducted at both room temperature and 77 K. A laser beam passing through two ground surfaces and two polished surfaces is depicted in Fig. 10. The scattering effect of the ground surface on the laser is evident.

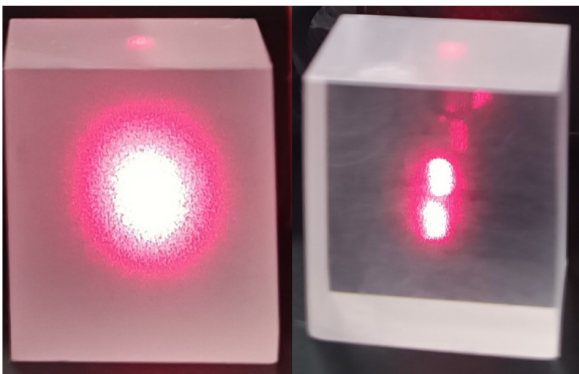


Fig. 10. A laser beam passing through two ground surfaces (left) and two polished surfaces (right)

Experiment B was identical to Experiment A except the crystals were cylindrical rather than cubic.

Experiments A and B compare different crystals. To eliminate differences between crystals, Experiments C and D were conducted. In Experiment C, a cubic crystal was initially ground and then polished, and the light yields were measured before and after the polishing process. Experiment D was identical to Experiment C, except another ground crystal was used. Experiments C and D were only conducted at room temperature.

Besides these four experiments with pCsI crystals, similar experiments were also conducted for CsI(Na) and CsI(Tl) crystals with the same procedure as Experiment C and D. The measured R_{ly} for these experiments are listed in Table 2.

As shown in Table 2, the light yields of ground crystals are consistently around 60–70% of the polished ones, regardless of temperature, crystal shape, or individual crystal. However, that ratios of CsI(Na) and CsI(Tl) are almost 1. Our hypothesis is that the UV light (310 nm at room temperature [35, 36] and 340 nm at 77 K [35]) emitted by pCsI is more

likely to be absorbed by the microstructures in the ground surface. In contrast, the light with longer wavelength emitted by CsI(Na) (420 nm [37, 38]) and CsI(Tl) (550 nm [39, 40]) is less susceptible to absorption by these microstructures. Although this hypothesis requires further verification, the results suggest that for future 10 kg pCsI detectors in the CLOVERS experiment, all crystal surfaces should be polished to achieve higher light yields.

Table 2. Ratio of the light yield (R_{ly}) between ground and polished crystals for different experiments. Defined in Eq.7

Experiment	pCsI(A)	pCsI(B)	pCsI(C)	pCsI(D)	CsI(Na)	CsI(Tl)
$R_{ly}(293K)$	0.68	0.62	0.63	0.68	0.94	1.0
$R_{ly}(77K)$	0.70	0.68	-	-	-	-

C. Influence of crystal shape on the light yield

The crystal shape may also influence the light yield, as indicated in Ref.[41] and Ref.[42]. A comparison between the light yield of cubic and cylindrical crystals was conducted, with both ground and polished crystals tested. The results are shown in Table 3. The light yields and energy resolutions of cubic crystals are slightly better than those of cylindrical crystals under both ground and polished conditions, but the difference is not significant. Therefore, in future CLOVERS experiments, the choice of crystal shape may depend on the shape of the photon detector to balance between light collection efficiency and detector mass. For instance, the crystal should be cuboid for SiPMs with square cathode regions and cylindrical for PMTs with circular cathode regions.

Table 3. Comparison of the light yield and energy resolution of crystals with different shapes and surface treatment.

Crystal	LY(PE/keV _{ee})	FWHM(%)
Cubic (polished)	35.2	6.9
Cubic (ground)	24.8	7.8
Cylindrical (polished)	33.9	7.1
Cylindrical (ground)	22.3	7.9

VI. SUMMARY

In this study, we conducted measurements of the light yield, energy resolution, and scintillation decay time of pCsI detectors at 77 K coupled with PMT HAMAMASTU R11065. We achieved a light yield of 35.2 PE/keV_{ee}, surpassing the assumed value for CLOVERS sensitivity estimation, and an unprecedented energy resolution of 6.9% FWHM at 60 keV, the best ever for cryogenic pCsI detector and world-leading for scintillation detectors. Improved light yield and resolution enhance sensitivity in CEνNS detection.

The shorter scintillation decay time of pCsI at 77 K compared to CsI(Na) at room temperature might strongly suppress the afterglow background from environmental radioactive events.

For optimizing the future CLOVERS 10 kg pCsI detector, we investigated the influence of temperature, surface treatment, and crystal shape. While the light yield peaks around 20 K, cooling a 10 kg material to 20 K is challenging. Since the light yield remains stable between 70 – 100 K, placing the pCsI in liquid argon at 87 K may be a more viable option, uti-

lizing liquid argon as an active veto system to mitigate outer background.

Surface treatment significantly impacts the light yield, with ground crystals yielding only 60 – 70 % of polished ones. Crystal shape, however, has minimal influence on the light yield. These findings suggest that for the future CLOVERS 10 kg pCsI detector, crystals should be polished and their shape should match the cathode area of photon detectors to maximize light yield and utilize the entire sensitive area of the photon detector.

-
- [1] D. Akimov, J. Albert, P. An, C. Awe, P. Barbeau, B. Becker, V. Belov, A. Brown, A. Bolozdynya, B. Cabrera-Palmer, *et al.*, *Science* **357**, 1123 (2017).
- [2] C. D. Ott, E. O'Connor, S. Gossan, E. Abdikamalov, U. Gamma, and S. Drasco, *Nuclear Physics B-Proceedings Supplements* **235**, 381 (2013).
- [3] I. Tamborra, F. Hanke, B. Müller, H.-T. Janka, and G. Raffelt, *Physical Review Letters* **111**, 121104 (2013).
- [4] Y. Huang *et al.*, (2024), [arXiv:2403.03566 \[nucl-ex\]](https://arxiv.org/abs/2403.03566).
- [5] K.-J. Kang *et al.* (CDEX), *Front. Phys. (Beijing)* **8**, 412 (2013), [arXiv:1303.0601 \[physics.ins-det\]](https://arxiv.org/abs/1303.0601).
- [6] X. Cao *et al.* (PandaX), *Sci. China Phys. Mech. Astron.* **57**, 1476 (2014), [arXiv:1405.2882 \[physics.ins-det\]](https://arxiv.org/abs/1405.2882).
- [7] F. An *et al.* (JUNO), *J. Phys. G* **43**, 030401 (2016), [arXiv:1507.05613 \[physics.ins-det\]](https://arxiv.org/abs/1507.05613).
- [8] C. Cai, G. Chen, J. Chen, F. Gao, X. Guo, T. He, C. Jia, G. Jin, Y. Jing, G. Ju, *et al.*, [arXiv preprint arXiv:2405.05554](https://arxiv.org/abs/2405.05554) (2024).
- [9] L. T. Yang, Y. F. Liang, and Q. Yue, *PoS TAUP2023*, 296 (2024).
- [10] C. Su, Q. Liu, and T. Liang (CLOVERS, CE ν NS@CSNS), *Phys. Sci. Forum* **8**, 19 (2023), [arXiv:2303.13423 \[physics.ins-det\]](https://arxiv.org/abs/2303.13423).
- [11] M.-Y. Huang, *Chinese Physics C* **40**, 063002 (2016), [arXiv:1507.08765 \[hep-ph\]](https://arxiv.org/abs/1507.08765).
- [12] A. Drukier and L. Stodolsky, *Physical Review D* **30**, 2295 (1984).
- [13] K. Ding, D. Chernyak, and J. Liu, *Eur. Phys. J. C* **80**, 1146 (2020), [arXiv:2008.00939 \[physics.ins-det\]](https://arxiv.org/abs/2008.00939).
- [14] K. Ding, J. Liu, Y. Yang, and D. Chernyak, *Eur. Phys. J. C* **82**, 344 (2022), [arXiv:2201.00483 \[physics.ins-det\]](https://arxiv.org/abs/2201.00483).
- [15] CAEN, “Caen wavedump,” (2024).
- [16] C. Su, “Wavedump ucas,” (2024).
- [17] C. Su, “Waveana,” (2024).
- [18] B. Scholz, *First observation of coherent elastic neutrino-nucleus scattering* (Springer, 2018).
- [19] L. E. S.Y.F. Chu and R. Firestone, “Www table of radioactive isotopes,” (2024).
- [20] L. Wang, G. d. Li, Z. Y. Yu, X. H. Liang, T. A. Wang, F. Liu, X. L. Sun, C. Guo, and X. Zhang, (2022), [arXiv:2212.11515 \[physics.ins-det\]](https://arxiv.org/abs/2212.11515).
- [21] R. Hawrami, E. Ariesanti, A. Farsoni, D. Szydel, and H. Sabet, *Crystals* **12**, 1517 (2022).
- [22] N. Yavuzkanat, M. Şenyiğit, and M. Kaplan, *Revista mexicana de física* **68** (2022).
- [23] R. Casanovas, J. Morant, and M. Salvadó, *Nuclear Instruments and Methods in Physics Research Section A: Accelerators, Spectrometers, Detectors and Associated Equipment* **675**, 78 (2012).
- [24] W. Chewpraditkul, L. Swiderski, and M. Moszynski, *Nukleonika* **53**, 51 (2008).
- [25] L. Swiderski, A. Gojska, M. Grodzicka, S. Korolczuk, S. Mianowski, M. Moszynski, J. Rzakiewicz, P. Sibezyński, A. Syntfeld-Kazuch, M. Szawłowski, *et al.*, in *Proceedings of the 1st EPS Conference on Plasma Diagnostics*. Available from http://pos.sissa.it/archive/conferences/240/162/ECPD2015_162.pdf (2015).
- [26] C. Amsler, D. Grögler, W. Joffrain, D. Lindelöf, M. Marchesotti, P. Niederberger, H. Pruyss, C. Regenfus, P. Riedler, and A. Rotondi, *Nuclear Instruments and Methods in Physics Research Section A: Accelerators, Spectrometers, Detectors and Associated Equipment* **480**, 494 (2002).
- [27] J. Liu, F. Liu, X. Ouyang, B. Liu, L. Chen, J. Ruan, Z. Zhang, and J. Liu, *Journal of Applied Physics* **113** (2013).
- [28] X.-L. Sun, J.-G. Lü, T. Hu, L. Zhou, J. Cao, Y.-F. Wang, L. Zhan, B.-X. Yu, X. Cai, J. Fang, *et al.*, *Chinese Physics C* **35**, 1130 (2011).
- [29] V. Mikhailik, V. Kapustyanyk, V. Tsybul'skiy, V. Rudyk, and H. Kraus, *physica status solidi (b)* **252**, 804 (2015).
- [30] C. Amsler, D. Grögler, W. Joffrain, D. Lindelöf, M. Marchesotti, P. Niederberger, H. Pruyss, C. Regenfus, P. Riedler, and A. Rotondi, *Nuclear Instruments and Methods in Physics Research Section A: Accelerators, Spectrometers, Detectors and Associated Equipment* **480**, 494 (2002).
- [31] X. Zhang, X. Sun, J. Lv, P. Lv, *et al.*, (2018).
- [32] A. Knyazev, J. Park, P. Golubev, J. Cederkäll, H. Alvarez-Pol, J. Benlliure, P. Cabanelas, E. Casarejos, L. Causeret, D. Cortina-Gil, *et al.*, *Nuclear Instruments and Methods in Physics Research Section A: Accelerators, Spectrometers, Detectors and Associated Equipment* **1003**, 165302 (2021).
- [33] I. Kilimchuk, V. Tarasov, and I. Vlasova, *Radiation Measurements* **45**, 383 (2010).
- [34] E. Roncali and S. R. Cherry, *Physics in Medicine & Biology* **58**, 2185 (2013).
- [35] C. L. Woody, P. Levy, J. Kierstead, T. Skwarnicki, Z. Sobolewski, M. Goldberg, N. Horwitz, P. Souder, and D. Anderson, *IEEE Transactions on Nuclear Science* **37**, 492 (1990).
- [36] G. Ren, C. Song, Z. Zhang, K. Zhang, F. Yang, H. Li, and X. Chen, *Journal of Inorganic Materials* **32**, 169 (2017).
- [37] F. Liu, X. Ouyang, M. Tang, Y. Xiao, B. Liu, X. Zhang, Y. Feng, J. Zhang, and J. Liu, *Applied Physics Letters* **102** (2013).
- [38] J.-C. Hsu and Y.-S. Ma, *Coatings* **9**, 751 (2019).
- [39] L. Guo, B. Jiang, C. Tian, P. Chen, and S. Liu, *Crystals* **13**, 1355 (2023).
- [40] C. Tian, S. Liu, Y. Xie, L. Guo, S. Zhang, Y. Liu, and Z. Zhong, *Journal of Materials Science: Materials in Electronics* **30**, 7691 (2019).

- [41] F. Danevich, V. Kobychev, R. Kobychev, H. Kraus, V. Mikhailik, V. Mokina, and I. Solsky, *Nuclear Instruments and Methods in Physics Research Section B: Beam Interactions with Materials and Atoms* **336**, 26 (2014).
- [42] M. Sasano, H. Nishioka, S. Okuyama, K. Nakazawa, K. Makishima, S. Yamada, T. Yuasa, A. Okumura, J. Kataoka, Y. Fukazawa, *et al.*, *Nuclear Instruments and Methods in Physics Research Section A: Accelerators, Spectrometers, Detectors and Associated Equipment* **715**, 105 (2013).